RSC Chemical Biology

ROYAL SOCIETY OF CHEMISTRY

PAPER

View Article Online
View Journal

Cite this: DOI: 10.1039/d6cb00070c

ortho-Substituents govern aryl aldehyde reactivity: toward lysine-targeted, tunable inhibitors of glucose-6-phosphate dehydrogenase

Bronwyn E. Rowland,[a] Kelsey D. Roy,[b] Adil Alkaş,[ab] Mirele Barsoum,[a] Tangweth Kuot,[b] Jesse C. Fuller,[a] Adrien J. Naudet,[c] Elisa Ospanow[a] and David L. Jakeman *[ab]

Certain drugs achieve highly potent and long-lasting enzyme inhibition by forming covalent bonds with nucleophilic amino acid functionalities. Aldehyde-containing inhibitors are able to react with lysine ε-amino functionalities to form reversible-covalent imine (Schiff base) adducts. *ortho*-Substituted aryl aldehydes have been used to further stabilize these imines through intramolecular interactions. However, relationships between aryl aldehyde structure, reactivity, and enzyme inhibition remain poorly defined. To address this gap, we characterized imine formation across a diverse panel of aryl aldehydes in aqueous solution and tested whether reactivity trends will predict covalent inhibition mechanisms. First, we assessed imine yield, reaction rate, and apparent binding affinity by NMR and UV-vis spectroscopy using a lysine surrogate. We then evaluated inhibitory activity against an enzyme using dose–response and dilution assays to determine potency and reversibility. *Leuconostoc mesenteroides* glucose-6-phosphate dehydrogenase (G6PD), which contains a lysine-rich active site, served as the enzyme model. The reactivity of aryl aldehydes in our panel was primarily governed by *ortho*-substituents, particularly their ability to stabilize the imine and coordinate the reacting partners. Reactivity generally correlated with inhibitor potency, but not with reversibility. We also identified previously unreported aryl aldehyde G6PD inhibitors bearing boronic acid, ethynyl, and phosphonate substituents, spanning irreversible-covalent, reversible-covalent, and rapid-equilibrium inhibition mechanisms. These findings establish structure–reactivity–activity relationships for aryl aldehydes and demonstrate their potential for tunability in rational inhibitor design. Collectively, this work strengthens the foundation for lysine-targeted covalent inhibitor development.

Received 23rd February 2026,
Accepted 6th May 2026

DOI: 10.1039/d6cb00070c

rsc.li/rsc-chembio

Introduction

Covalent drug discovery is undergoing a renaissance.[1–5] These agents achieve potent and sustained inhibition by forming a covalent bond with a specific amino acid in a targeted protein. Several widely used drugs, including aspirin, penicillin, cephalosporins, and proton pump inhibitors, act through a covalent mechanism, although this was only recognized post-discovery. Afatinib and ibrutinib were among the first rationally designed covalent drugs, developed to target tumour-promoting (oncogenic) protein kinases.[3] These drugs demonstrated that covalent inhibitors can be structurally optimized to control reactivity, addressing previous therapeutic concerns of promiscuity or toxicity. The pharmacodynamics of a covalent drug, including its potency and reversibility, are highly dictated by its electrophilic "warhead",[1] the functional group responsible for covalent binding to the targeted amino acid nucleophile (Fig. 1). "Electrophile-first" approaches to covalent drug design have, therefore, become increasingly common, in which

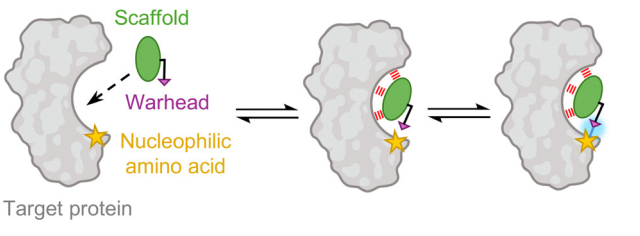

Fig. 1 Binding mechanism and structural components of a covalent inhibitor. The inhibitor scaffold forms initial non-covalent interactions (red dashed lines). The warhead subsequently forms a covalent bond (highlighted blue line) with a proximal amino acid.

[a] Department of Chemistry, Dalhousie University, Halifax, Nova Scotia B3H 4R2, Canada. E-mail: david.jakeman@dal.ca
[b] College of Pharmacy, Dalhousie University, Halifax, Nova Scotia B3H 4R2, Canada
[c] Faculté de Pharmacie, Université Grenoble Alpes, Grenoble 38400, France

reactive covalent fragments are identified first, followed by installation of the non-covalent scaffold.[3,6] This approach enabled the discovery of sotorasib as an inhibitor for $KRAS_{G12C}$, an oncogenic protein previously considered "undruggable".[7] Reversible-covalent warheads have gained particular attention as they may combine the respective advantages of covalent and non-covalent inhibition by maintaining prolonged residence times with the target, while allowing rapid dissociation of non-specific interactions.[1,8–10]

Cysteine amino acids are the most common targets for covalent modification due to the nucleophilicity of their thiol side-chains.[1,11] However, cysteines are rare within protein sequences, leading to the exploration of other nucleophilic targets, including serine, glutamate, and lysine side-chains.[2] Although lysine ε-NH_2 groups (pK_a = 10–11) are relatively weak nucleophiles at physiological pH (7.4), local pK_a shifts within a protein binding pocket, together with a small amine-aldehyde orbital energy gap (HOMO–LUMO gap) often help promote imine formation.[12,13] A range of lysine-targeting warheads have been investigated, including sulfur(VI) fluoride electrophiles,[14–16] *N*-acyl-*N*-alkyl sulfonamides,[17,18] nitriles,[19,20] and activated esters.[21,22] Lysine ε-NH_2 groups can also undergo reversible-covalent modification through condensation with an aldehyde or ketone to form an imine (C═N, Schiff base). Aldehyde-based electrophiles have been developed into amine-targeting covalent probes,[23,24] labels,[25,26] and inhibitors.[27–32] In addition, pyridoxal 5′-phosphate-dependent enzymes form imines as part of their catalytic mechanism.[33]

A central challenge for aldehyde-based inhibitors using imine chemistry is competition with water. Imines are prone to hydrolysis and aldehydes to hydration, both of which decrease the thermodynamic favourability of adduct formation (Fig. 2A). To shift the equilibria toward the imine, the aldehyde is often installed onto an aromatic ring with an *ortho*-substituent capable of forming a stabilizing intramolecular interaction. For example, salicylaldehydes stabilize imines through hydrogen bonding,[34] whereas 2-carbonylphenylboronic acids form a N–B dative bond (Fig. 2B).[35] Some *ortho*-substituents with a lone pair of electrons stabilize adducts through donation of electron density to the imine carbon (n → π* orbital interactions), as shown for 2-carboxybenzaldehyde.[36] In contrast, 2-ethynylbenzaldehydes react with lysine ε-NH_2 to form imines that undergo an intramolecular tandem cyclization, yielding stabilized, albeit irreversible isoquinolinium adducts.[27,37] More recently, chalcogen bonds involving sulfur, selenium, or tellurium have also been shown to stabilize imines in aqueous media.[38]

Despite a strong understanding of imine chemistry and its application to reversible-covalent enzyme modification, it remains unclear how solution-phase reactivity translates into covalent enzyme inhibition, and ultimately, therapeutic performance. First, there are few standardized structure–reactivity relationship studies across broad panels of *ortho*-substituted aryl aldehydes. Existing reports show that both the stabilization mechanism and the steric and electronic properties of the *ortho*-substituent influence imine formation by affecting aldehyde binding affinity, reaction rate, adduct stability, or susceptibility to competing hydration reactions.[13,35,36,39–44] However, comparisons across studies are difficult because experimental conditions vary. Second, despite the prevalence of targetable lysine residues in proteins,[45–48] systematic investigations of aldehyde-mediated enzyme inhibition are limited. As a result, predicting imine formation under biologically relevant conditions remains challenging, hindering the rational selection of warheads for lysine-targeting covalent inhibitors.

To address this gap, we first benchmarked substituent effects on imine formation using a lysine surrogate, establishing trends in imine yield, reaction rate, and apparent binding affinity across a diverse panel of aryl aldehydes. We then tested

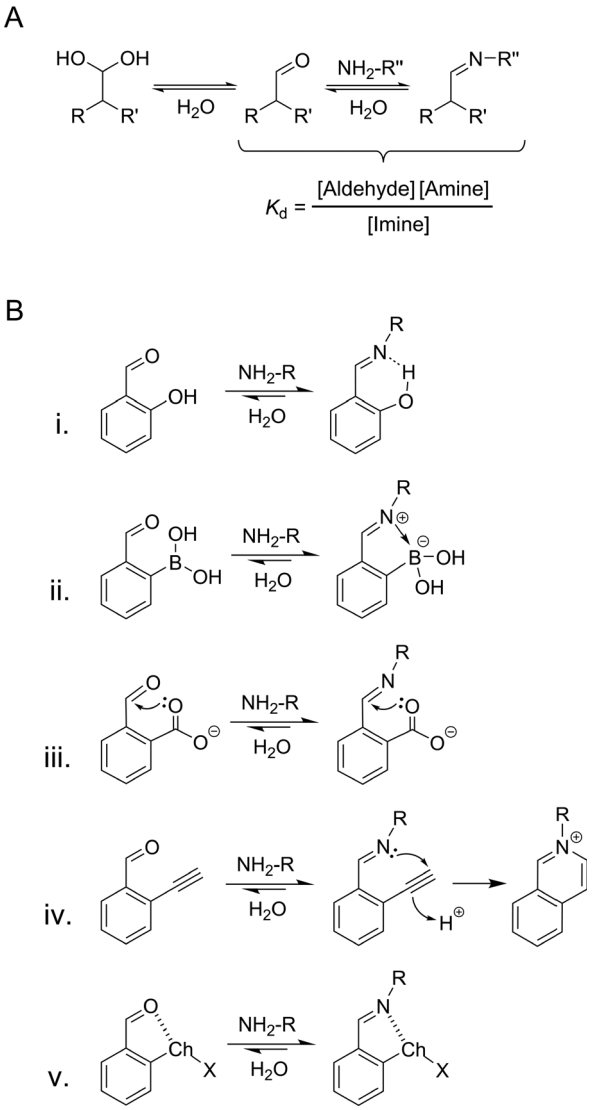

Fig. 2 (A) Aldehyde hydration and imine formation equilibria. (B) Intramolecular imine stabilization by *ortho*-substituted aryl aldehydes: (i) salicylaldehyde hydroxyl group participates in hydrogen bonding; (ii) boronic acid substituent of 2-formylphenylboronic acid forms an N–B dative bond; (iii) 2-carboxybenzaldehyde stabilizes open forms of aldehyde and imine through n → π* orbital interactions *via* its carboxyl substituent; (iv) alkynyl group of 2-ethnylbenzaldehyde drives tandem cyclization of imine to afford isoquinolinium species; (v) aryl aldehydes with *ortho*-chalcogen groups (Ch–X: Ch = S/Se/Te, X = Me/Ph) participate in chalcogen bonding.

whether these trends predict enzyme inhibition mechanisms using *Leuconostoc mesenteroides* glucose-6-phosphate dehydrogenase (G6PD) as an exploratory model. Our results reveal broad physicochemical and pharmacodynamic diversity among the tested aryl aldehydes, largely governed by *ortho*-substituents. We also identified electrophiles with previously unreported activity against G6PD. The functional tunability of these aldehydes supports an electrophile-first design strategy, in which *ortho*-substitution may serve to modulate inhibitor reactivity, potency, and reversibility. These findings frame *ortho*-substituted aryl aldehydes as a potentially versatile platform for meeting diverse pharmacological goals.

Materials and methods

General methods and instrumentation

All chemicals were obtained from Sigma-Aldrich and used without further purification unless otherwise stated. The following compounds were purchased from Combi-Blocks: 4-pyridinecarboxaldehyde, 2-acetylphenylboronic acid, benzaldehyde-2,4-disulfonic acid, 2-formylbenzenesulfonic acid, 2-carboxybenzaldehyde, 2-ethynylbenzaldehyde, and 3-formyl-4-hydroxybenzoic acid. 2-Formylphenylboronic acid and N^{α}-(*tert*-butoxycarbonyl)-L-lysine (Boc-Lys) were obtained from AstaTech. *Leuconostoc mesenteroides* α-D-glucose-6-phosphate dehydrogenase (G6PD) (Product No. 10165875001, EC 1.1.1.363) was prepared as a stock solution (200 U mL^{-1}) in enzyme assay buffer containing glycerol (50% v/v), and stored at −20 °C. The assay buffer consisted of 3-(*N*-morpholino)propanesulfonic acid (MOPS, 40 mM) in Millipore water, adjusted to pH 7.4. Working solutions of G6PD were prepared immediately prior to use. UV-Vis absorbance and pathlength were measured in 96-well flat-bottom microtiter plates (Corning Costar) on a SpectraMax Plus 384 UV-vis microplate reader using the PathCheck feature and SoftMaxPro 4.6 software. A Sentron (Millar) SI series MicroFET pH/T probe was used to measure pH. For characterizing imine formation, ^{1}H NMR spectra were recorded in 5 mm NMR tubes on a Bruker Avance Neo-400 spectrometer (400 MHz) and processed using TopSpin 4. Spectra were referenced to the resonance of D_2O (δ = 4.69 ppm) as an internal standard and phase-adjusted prior to integration. Regression analyses and data plotting were performed using GraphPad Prism 10.1.1.

Synthetic procedures

Experimental details for the synthesis and characterization of 2-formylphenylphosphonic acid (**11**) and (2-formylphenyl)(methyl)diphenylphosphonium iodide (**12**) are provided in the SI (Fig. S1–S10).

Characterization of imine formation by ^{1}H NMR spectroscopy

NMR experiments were performed as previously described,[40] with minor modifications. Samples (500 μL total) were prepared by mixing 140 μL D_2O, 10 μL aryl aldehyde (0.1 M in DMSO-d_6), and 100 μL Boc-Lys (0.1 M in D_2O) in 250 μL phosphate buffered saline (PBS, 0.1 M in D_2O). The pH of the PBS was approximately ∼7.3, adjusted to account for the use of deuterated solvent.[49] Final concentrations were 2 mM aryl aldehyde, 20 mM Boc-Lys, and 50 mM PBS. Mixtures were incubated at room temperature and allowed to equilibrate before acquisition of ^{1}H NMR spectra (512 scans, SW = 12 ppm, D1 = 1.5 s, O1P = 6 ppm). The spectra for most compounds were recorded after 2–6 hours of incubation, except compound **7**, which was analyzed after 24 hours due to slow equilibration. Control samples lacking either aldehyde or Boc-Lys (replaced with D_2O, Fig. S11) were prepared and analyzed under identical conditions.

Relative integration values were used to calculate the proportion of aldehyde/ketone, imine, and hydrate in each sample. Fig. S12 illustrates the calculation procedure used for aldehydes. An alternative procedure was used for the ketone 2-acetylphenylboronic acid (**6**, calculation described in Fig. S13).

Characterization of imine formation by UV-vis spectroscopy

Stock solutions of aldehyde (1 mM) and Boc-Lys (100 mM) were prepared in PBS (pH 7.4) and adjusted to pH 7.4. A minimal amount of DMSO was added to the aldehyde stocks if necessary for solubilization. Solution A (1 mM aldehyde) and solution B (1 mM aldehyde and 100 mM Boc-Lys) were prepared in PBS. In a microtiter plate, solution A and B were mixed in the appropriate volumes to give 8 reactions (200 μL) containing 1 mM aldehyde with 100 mM, 60 mM, 40 mM, 20 mM, 10 mM, 5 mM, 2 mM, or 0 mM Boc-Lys. Reactions were monitored using a microplate reader, measuring the spectra (250–800 nm, 10 nm increments) at 0, 1, 2, 4, and 24 h post-initiation. A plate well containing 200 μL PBS was used as a blank. Between readings, the microplate was left to react at room temperature and sealed to minimize evaporation.

The apparent association constant (K_a^{app}) at each timepoint was determined using the online software BindFit v0.5.[50,51] The spectra were fit to a 1 : 1 binding model represented by eqn (1), where [A] is the concentration of aldehyde, [B] is the concentration of Boc-Lys, and [AB] is the concentration of aldimine. Fitting the entire spectrum rather than selecting a single wavelength provides a more accurate fit.[51] When no reaction was observed between Boc-Lys and the aldehyde (*i.e.* no spectral shift), K_a^{app} was not calculated. Apparent dissociation constants (K_d^{app}) were calculated from K_a^{app} values according to eqn (2).

$$K_a^{app} = \frac{[AB]}{[A][B]} \quad (1)$$

$$K_d^{app} = \frac{1}{K_a^{app}} \quad (2)$$

G6PD kinetic parameters

G6PD activity was measured using a continuous, spectrophotometric assay adapted from our previous work.[52] To determine the apparent binding affinity (K_m^{app}) to G6P, reactions were prepared in enzyme assay buffer containing 0.01 U mL^{-1} G6PD, 0.1 mM $NADP^+$, and serially diluted G6P (2-fold, 2 mM to ∼30 μM). Reactions (200 μL) were initiated with G6PD and monitored in a microtiter plate at 340 nm every 20 s (25 °C,

30 min total). The same procedure was used to determine the $NADP^+$ K_m^{app}, with reactions instead containing 1 mM G6P, and serially diluted $NADP^+$ (2-fold, 200 μM to ~3 μM). The Beer–Lambert Law was used to calculate the concentration of NADPH produced at each timepoint given the measured absorbance and pathlength of each well, and the known extinction coefficient of NADPH (6.22 mM^{-1} cm^{-1} at 340 nm). NADPH concentrations were normalized by subtracting the background concentration at t = 0 min. Initial velocities (v_i) were derived by linear regression of the first 3 minutes of the reaction and Michaelis–Menten curves were plotted. Duplicate experiments were fit to eqn (3) to calculate K_m^{app}, where [NADPH] is the concentration of NADPH formed, V_{max}^{app} is the apparent maximum velocity, and [S] is the concentration of G6P or $NADP^+$.

$$[\mathrm{NADPH}] = \frac{V_{max}^{app}[\mathrm{S}]}{K_m^{app} + [\mathrm{S}]} \quad (3)$$

Inhibition of G6PD: progress curves

Stock solutions of aldehydes were prepared in enzyme assay buffer or in assay buffer supplemented with 25% v/v DMSO if required for solubilization, and adjusted to pH 7.4 as necessary. These stocks were serially diluted in enzyme assay buffer (or assay buffer with 25% DMSO) to produce working solutions at 10× the desired final concentration. Assay buffer (150 μL), a 20× mixture of G6P and $NADP^+$ (10 μL), and the serial dilutions (20 μL) were mixed in a microtiter plate. A control well was included in each experiment, where the aldehyde was substituted with the appropriate vehicle. Reactions were initiated with 10× G6PD (20 μL) and monitored at 340 nm every 30 s (25 °C, 80 min total). Final concentrations were 0.001 U mL^{-1} G6PD, 100 μM $NADP^+$, 500 μM G6P, in either 0% or 2.5% DMSO. The concentration of NADPH at each timepoint was calculated as described (*vide supra*).

Inhibition of G6PD: jump dilutions

Inhibitor concentrations corresponding to approximately 10% G6PD inhibition (IC_{10}) were estimated from the collected progress curves and verified experimentally. Each aldehyde was incubated at 50× its estimated IC_{10} with 0.025 U mL^{-1} G6PD in enzyme assay buffer (30 min, r.t.). The incubation mixture also contained 25% DMSO as high-concentrate aldehyde stocks were necessary and DMSO aided in their solubilization. An aliquot of the incubation mixture (4 μL) was added to a microtiter plate and then rapidly diluted 50-fold with a ~1.02× mixture of G6P and $NADP^+$ in assay buffer (196 μL). Reactions were monitored at 340 nm every 30 s (25 °C, 130 min total). Final concentrations were 0.0005 U mL^{-1} G6PD, 100 μM $NADP^+$, 500 μM G6P, and 0.5% DMSO, with the aldehyde at its estimated IC_{10}. The concentration of NADPH at each timepoint was calculated as described (*vide supra*).

Dissociation rate constants (k_{-2}) were calculated for inhibitors showing reversible-covalent binding (nonlinear jump dilution curves) using eqn (4),[53] where [NADPH] is the concentration of NADPH formed, v_i is the initial velocity, v_s is the steady-state velocity, and t is the reaction time. Note that k_{-2} is also referred to as k_{off} in literature.[53] The value for v_s is constrained to 90% of the velocity of the uninhibited control (v_{ctrl} = 0.1192 μM min^{-1}, obtained by linear regression).[53] The v_i of very slow-dissociating inhibitors (compounds **2** and **4**) were calculated separately by linear regression of the first 60 min of the reaction. Otherwise, we found curve fitting to be unreliable given the limited dissociation observed within the experimental timeframe.

$$[\mathrm{NADPH}] = v_s t + \frac{v_i - v_s}{k_{-2}}\left(1 - e^{-k_{-2}t}\right) + 1 \quad (4)$$

Calculation of inhibition constants: reversible inhibitors

The inhibition mechanism of each compound was inferred from its progress curve shape and jump dilution behaviour (irreversible-covalent, reversible-covalent, or rapid-equilibrium). The progress curves of reversible-covalent inhibitors were fit to eqn (5)[54] to obtain v_i, v_s, and the observed rate constant (k_{obs}). Since [NADPH] was normalized to the background, the y-intercept ($Y0$) variable was constrained to 0. Rapid-equilibrium inhibitors and uninhibited control reactions were fit by linear regression to obtain v_i and v_{ctrl}, respectively, with $Y0$ constrained to 0 as well.[55]

$$[\mathrm{NADPH}] = v_s t + \frac{v_i - v_s}{k_{obs}}\left(1 - e^{-k_{obs}t}\right) + Y0 \quad (5)$$

The inhibition constants of compounds with a reversible binding mechanism were calculated from their fitted velocities. This method is generally more reliable and less error-prone than extracting inhibition constants from k_{obs} plots.[54] For reversible-covalent inhibitors, v_s values were normalized to v_{ctrl} and plotted on a log scale. Similarly, v_i values were normalized to v_{ctrl} and plotted in the same way for rapid-equilibrium inhibitors. K_x^{app} values were calculated from the plots according to eqn (6),[54] where [I] is the inhibitor concentration, h is the Hill slope, and v_x is either v_s or v_i. K_x^{app} represents the apparent inhibition constant (K_i^{app} for rapid-equilibrium and K_i^{*app} for reversible-covalent inhibitors). Note that this equation is equivalent to an IC_{50} determination with the top and bottom of the curve normalized to 100% and 0% activity, respectively.

$$\frac{v_x}{v_{ctrl}} = \frac{1}{1 + 10^{(\log K_x^{app} - \log[\mathrm{I}])h}} \quad (6)$$

True inhibition constants were estimated from the apparent values using eqn (7),[56] where [G6P] is the concentration of glucose-6-phosphate used in the assay, K_m^{app} is the apparent binding affinity of G6PD to G6P, and K_x is the true inhibition constant (K_i or K_i^*). This equation assumes that the inhibitors function by competing with G6P binding at the G6PD active site.

$$K_x = \frac{K_x^{app}}{1 + \frac{[\mathrm{G6P}]}{K_m^{app}}} \quad (7)$$

Calculation of inhibition constants: irreversible inhibitors

Irreversible-covalent inhibitors were identified by a lack of recovery in G6PD activity following jump dilution (compound **7**), and processed as described by Mader *et al.*[8] The end-point

concentrations of formed NADPH were calculated from the inhibitor progress curves at 15 timepoints, sampled every 5 min between 10–80 min of reaction time. These concentrations were plotted as a logarithmic dose–response curve, and time-dependent IC_{50} values ($IC_{50(t)}$) were calculated according to eqn (8), where $[NADPH]_{I(t)}$ and $[NADPH]_{ctrl(t)}$ are the concentrations of NADPH produced at a given timepoint in the inhibited and uninhibited reactions, respectively, [I] is the inhibitor concentration, and h is the Hill slope. This equation is analogous to eqn (6). Next, $IC_{50(t)}$ was plotted as a function of time and fit to eqn (9) to derive the apparent inhibition constant (K_I^{app}), where k_2 is the rate of inactivation and t is the reaction time. The true inhibition constant K_I was determined using eqn (7). Note that for irreversible-covalent inhibitors, k_2 is also referred to as k_{inact} in literature.[54]

$$\frac{[NADPH]_{I(t)}}{[NADPH]_{ctrl(t)}} = \frac{1}{1 + 10^{(\log IC_{50(t)} - \log[I])h}} \quad (8)$$

$$IC_{50(t)} = K_I^{app}\left(\frac{2 - 2e^{\frac{-k_2(IC_{50(t)})t}{IC_{50(t)} + K_I^{app}}}}{\frac{-k_2(IC_{50(t)})t}{IC_{50(t)} + K_I^{app}}} - 1\right) \quad (9)$$

Estimation of lysine residue pK_as

Amino acid pK_a values for *L. mesenteroides* G6PD were estimated using the online tool PypK_a, employing the pKAI prediction model.[57,58] A ligand-free crystal structure of *L. mesenteroides* G6PD, sourced from RCSB Protein Data Bank (PDB) (1H9B),[59] was used as the structural input. A pH range of 0–16 was evaluated using default model parameters.

Molecular modelling

A crystal structure of *L. mesenteroides* G6PD co-crystallized with G6P substrate was sourced from RCSB PDB (1E77).[59] MolSoft ICM-Browser was used for protein structure visualization.

Results

We designed a two-part system to evaluate aryl aldehyde imine formation and enzyme inhibition. First, we probed the reactivity of a panel of aryl aldehydes using a lysine surrogate, establishing physicochemical trends controlling imine yield, reaction rate, and apparent binding affinity. We then evaluated whether the established trends also determine pharmacodynamic outcomes in terms of aryl aldehyde potency and reversibility as inhibitors against *L. mesenteroides* glucose-6-phosphate dehydrogenase (G6PD). Fig. 3 shows the selected panel of aryl aldehydes, consisting of commercially sourced benzaldehyde (**1**), 4-pyridinecarboxaldehyde (**2**), and common *ortho*-substituted analogues **3–10**, together with phosphonate- or phosphonium-substituted derivatives synthesized in-house (**11**, **12**). These compounds were chosen based on their prevalence in literature, accessibility, and documented ability to form imines,[13,23,35,36,39,40,60–63] with benzaldehyde serving as a reference compound. This panel includes one aryl ketone (**6**) as this compound is commonly studied alongside its aldehyde analog (**5**) and has been used successfully in lysine-targeted protein modification.[25,35,64] However, we will refer to all compounds as aldehydes for ease of discussion.

Reactivity of aryl aldehydes with Boc-Lys

N^{α}-(*tert*-Butoxycarbonyl)-L-lysine (Boc-Lys) was used as a lysine surrogate as it closely matches the structure and basicity of lysine (pK_a = ~10.5). Some studies use more acidic amines, such as aniline or cholamine (pK_a = 5.3 and 7.9, respectively),[13,39] to mimic the perturbation of lysine pK_a that can occur within enzyme binding pockets due to solvent seclusion or proximal cationic residues.[12,65,66] However, we were motivated to use Boc-Lys since these pK_a shifts can vary widely across proteins and are often challenging to measure using techniques such as protein NMR. Furthermore, although a pK_a < 8.4 is commonly used to define targetable lysine residues,[67] exceptions to this rule exist. The catalytic lysine in phosphatidylinositol-3-kinase-δ has been successfully modified despite an estimated pK_a of 10.5–11.5, with deprotonation proposed to occur through water-mediated proton transfer.[22,68] We note that reactivity studies with amino acid

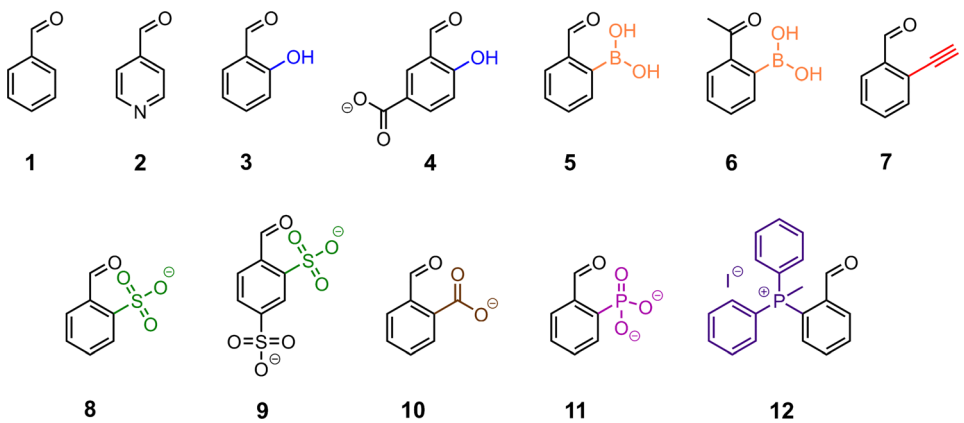

Fig. 3 Chemical structures of aryl aldehydes studied in this work. *ortho*-Substituents are grouped and distinguished by colour (blue = hydroxyl, orange = boronic acid, red = ethynyl, green = sulfonate, brown = carboxylate, pink = phosphonate, purple = phosphonium).

surrogates such as Boc-Lys cannot capture constraints imposed by a protein binding pocket, including limits on electrophile size and orientation, or the catalytic role of any ordered water molecules.[68–70] These studies, therefore, prioritize the identification of strong electrophiles that modify solvent-exposed or weakly nucleophilic residues, such as N-terminal or surface residues. Imine formation between Boc-Lys and compounds **1–12** were assessed in aqueous buffered solution (pH 7.4) by NMR spectroscopy. The proportion of imine formed after equilibrium was used as a measure of reactivity (Fig. 4). 2-Ethynylbenzaldehyde (**7**) produced the highest adduct levels (63%). 2-Carbonylphenylboronic acids **5** and **6** gave moderate yields (43% and 36%, respectively), followed by salicylaldehydes **3** and **4** (36% and 16%, respectively) (Fig. S16–S20). *ortho*-Sulfonate-substituted aryl aldehydes (**8**, **9**) showed very low imine yields (<1%) (Fig. S21 and S22). The remaining aldehydes (**1**, **2**, **10–12**) showed no detectable imine formation with Boc-Lys (Fig. S14, S15, S23–S25). These compounds either lack an *ortho*-substituent or contain charged functional groups. Aldehyde hydration, which competes with imine formation, was substantial only for 4-pyridinecarboxaldehyde (**2**). In contrast to benzaldehyde (**1**), which was inert, more than 50% of this pyridine derivative underwent hydration.

Imine formation was further evaluated by UV-vis spectroscopy to monitor adduct formation, persistence, and to estimate binding affinity. Although NMR spectroscopy could provide similar information, it requires more material and longer acquisition times. Absorption spectra were recorded for reaction mixtures of aryl aldehyde and various concentrations of Boc-Lys at 0, 1, 2, 4, and 24 h (Fig. 5 and S26). Amine-dependent spectral shifts were observed for compounds **3–7**, consistent with a reaction with Boc-Lys. The dissociation constants (K_d^{app}) of these compounds were calculated using BindFit[50,51] (Table 1) to monitor apparent binding affinity over time (Fig. 2A). This parameter is reported as an apparent value to account for time-dependent adduct formation and persistence, as well as the potential for competing pathways, such as aldehyde hydration, to affect the equilibrium.[71,72] 2-Carbonylphenylboronic acids (**5**, **6**) showed stable K_d^{app} values over 24 h, suggesting rapid and stable imine formation. These compounds also exhibited the lowest K_d^{app} values, and therefore strongest apparent binding affinity, across all timepoints (~4–5 mM). Comparatively, 3-formyl-4-hydroxybenzoic acid (**4**) required an hour to reach equilibrium and the apparent binding affinity was about 2-fold weaker (K_d^{app} = 9–11 mM). In contrast, **3** and **7** did not establish a clear equilibrium. Both aldehydes approached a minimum K_d^{app} of ~24 mM within 1 h, followed by a gradual increase over the next 23 hours, suggesting additional reaction pathways compete with imine formation. For compound **7**, an increase in aromatic proton count (Fig. S20) and a concentration-dependent colour change from clear to dark blue (Fig. S27) supported the formation of an isoquinolinium species rather than a simple imine.[73]

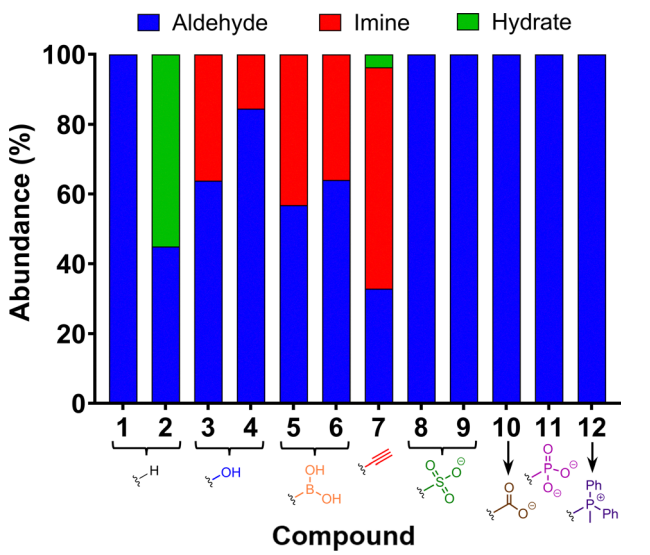

Fig. 4 Proportion of aldehyde, hydrate, and imine in reaction mixtures of compounds **1–12** (2 mM) and Boc-Lys (20 mM). The corresponding *ortho*-substituent is indicated below each compound number. Reactions conducted in PBS (pH 7.4) at room temperature and spectra recorded at reaction equilibrium. Percent abundance calculated from relative NMR integration of one experimental replicate (Fig. S12 and S13).

Mechanisms of aryl aldehyde inhibition of G6PD

To determine whether *ortho*-substituent effects translate to inhibition mechanism, we evaluated aryl aldehydes as electrophilic warheads against *L. mesenteroides* G6PD, a relevant yet underexplored enzyme model. G6PD catalyzes the conversion of glucose-6-phosphate (G6P) to 6-phosphogluconolactone, coupled to the reduction of $NADP^+$ (Fig. 6A).[74] The active site of *L. mesenteroides* G6PD contains five lysine residues potentially capable of covalent modification (Fig. 6B).[75] This reactivity is supported by studies showing that pyridoxal 5′-phosphate (PLP), a salicylaldehyde derivative, competes with G6P by forming a reversible-covalent imine bond to a lysine residue in the enzyme active site (Fig. 6C).[76,77]

Enzyme activity was quantified by measuring NADPH production using a continuous, spectrophotometric assay. Since G6P and $NADP^+$ bind *L. mesenteroides* G6PD with high affinity (K_m^{app} ~ 100 μM and ~10 μM, respectively, Fig. S28 and Table S1), they were used at 5× and 10× their respective K_m^{app} values to generate a quantifiable signal. Under these assay conditions, G6PD was tolerant of up to 2.5% DMSO without loss of rate (Fig. S29A). Inhibition reactions were therefore run with a final concentration of 2.5% DMSO or no DMSO if the solubility of the aldehyde allowed. However, all quantitative analyses were normalized to an appropriate control (containing either 2.5% or 0% DMSO), mitigating potential solvent-dependent effects.

Inhibition progress curves were generated by measuring G6PD activity across varying concentrations of aryl aldehyde. Concentrations were selected based on the individual potency and solubility limit of each compound. The shape of the progress curves varied across the aldehydes, indicating different inhibition mechanisms (Fig. 7).[78–80] Compounds **1**, **3**, **6**, and **8** produced linear curves of roughly constant initial velocity (v_i), consistent with a rapid establishment of the

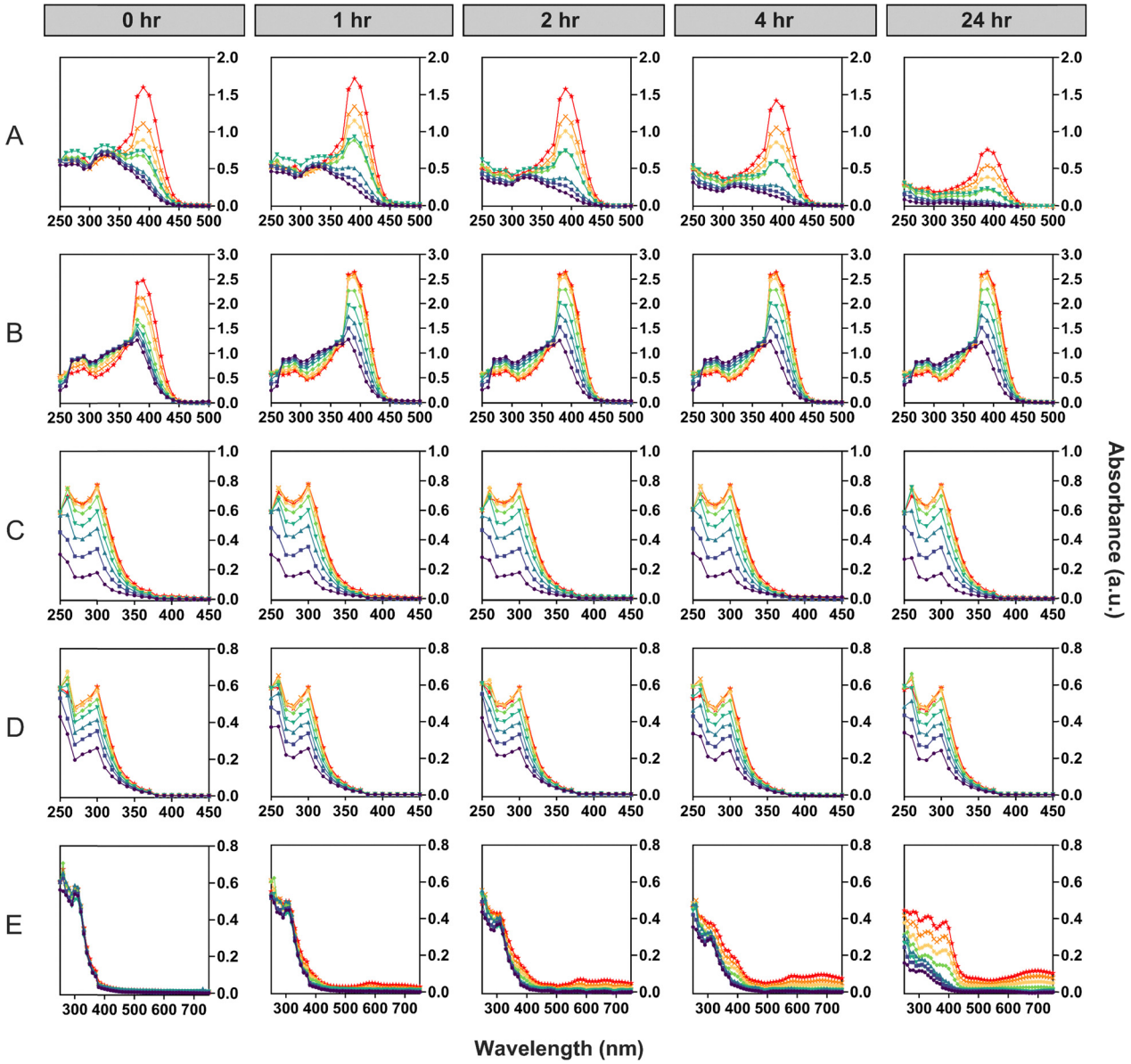

Fig. 5 Spectrophotometric titrations of Boc-Lys with (A) salicylaldehyde (**3**), (B) 3-formyl-4-hydroxybenzoic acid (**4**), (C) 2-formylphenylboronic acid (**5**), (D) 2-acetylphenylboronic acid (**6**), and (E) 2-ethynylbenzaldehyde (**7**). Reaction mixtures contained 1 mM aryl aldehyde with 100 mM (★), 60 mM (✕), 40 mM (✳), 20 mM (◆), 10 mM (▼), 5 mM (▲), 2 mM (■), or 0 mM (●) Boc-Lys in PBS (pH 7.4). Reactions conducted at room temperature and spectra recorded at 0, 1, 2, 4, and 24 h post-initiation. Data shown correspond to one replicate.

enzyme–inhibitor equilibrium. This behaviour is typical of reversible non-covalent inhibition, although a labile reversible-covalent bond sometimes results in similar kinetics.[78,79] Conversely, compounds **2**, **4**, **5**, **7**, **9** and **10** produced biphasic curves, indicative of time-dependent, covalent binding.[80] These curves are characterized by an initial velocity (v_i), followed by a

Table 1 Apparent dissociation constants of imine formation with Boc-Lys

	K_d^{app} [a] (mM)				
Aryl aldehyde	0 h	1 h	2 h	4 h	24 h
3	142.7 (± 4.8)	23.6 (± 1.2)	32.2 (± 1.3)	41.7 (± 1.5)	55.9 (± 2.4)
4	79.4 (± 1.8)	11.5 (± 0.3)	9.6 (± 0.3)	9.5 (± 0.2)	9.3 (± 0.2)
5	4.1 (± 0.2)	4.4 (± 0.2)	4.3 (± 0.2)	4.7 (± 0.2)	3.8 (± 0.2)
6	4.0 (± 0.2)	4.7 (± 0.2)	5.2 (± 0.2)	5.1 (± 0.2)	4.7 (± 0.2)
7	n.r.[b]	25.4 (± 3.0)	32.9 (± 2.9)	61.0 (± 3.5)	88.6 (± 2.4)

[a] Data reported as parameter estimates ± SE, derived from nonlinear least-squares regression of one experimental replicate. [b] n.r. = no reaction.

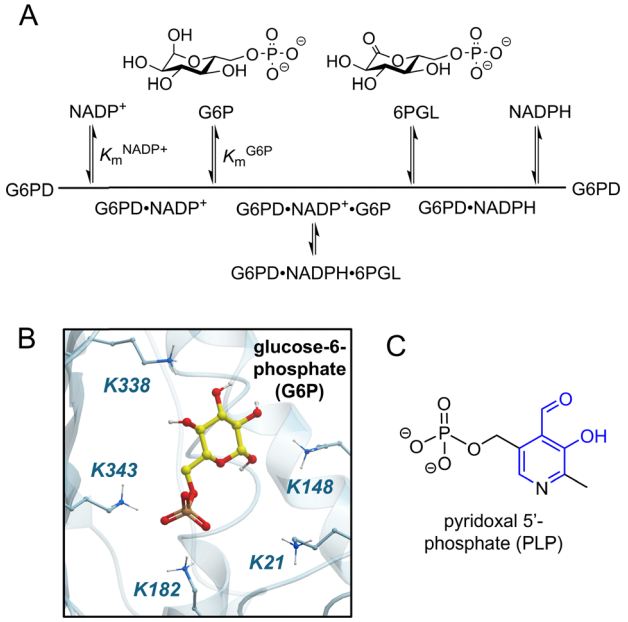

Fig. 6 (A) Cleland diagram of the ordered sequential Bi–Bi mechanism of G6PD catalysis. Coenzyme $NADP^+$ binds first, followed by glucose-6-phosphate (G6P). After catalysis, the product 6-phosphogluconolactone (6PGL) is released prior to NADPH. (B) G6P substrate bound to active site of *L. mesenteroides* G6PD (PDB: 1E77).[75] Lysine residues present in the active site are indicated. (C) Structure of G6PD inhibitor pyridoxal 5′-phosphate. Salicylaldehyde parent structure is highlighted in blue.

lower steady-state velocity (v_s). Irreversible-covalent inhibition results in $v_s = 0$ due to permanent deactivation of the enzyme, whereas reversible-covalent inhibition maintains residual activity such that $v_s \neq 0$, $v_s < v_i$. However, slow-binding reversible-covalent inhibition is often difficult to distinguish from true irreversible inhibition based on curve shape alone.[81] Finally, the phosphonate-substituted aryl aldehyde (**11**) yielded ambiguous curve shapes, prompting further investigation, and the phosphonium-substituted aryl aldehyde (**12**) showed little inhibitory activity. Inhibition by compound **10** was limited within its range of solubility.

Jump dilution experiments were performed to further assess inhibitor reversibility and better distinguish between inhibition mechanisms. G6PD was pre-incubated with a high concentration of aldehyde and then rapidly diluted with substrate, simultaneously initiating the reaction and reducing the effective inhibitor concentration from 100% to ~10% (Fig. S30 and Table S2). To aid in aldehyde solubility, all pre-incubation mixtures contained 25% DMSO. Reaction initiation involved a 50-fold dilution, lowering the DMSO concentration from 25% to a negligible 0.5%, with no observed effect on G6PD activity (Fig. S29B). Compound **10** was excluded from these experiments due to limited solubility at the required concentration.

These experiments showed varying degrees of reversibility among the aryl aldehydes (Fig. 8). For compounds **1**, **3**, **5**, **6**, and **8**, G6PD activity was recovered almost immediately upon dilution, suggesting rapid dissociation of inhibitor from the enzyme. With the exception of **5**, each of these compounds also displayed rapid association of enzyme and inhibitor, as previously indicated by their linear progress curves (Fig. 7). 2-Ethynylbenzaldehyde (**7**) demonstrated irreversible binding as no enzyme activity was regained after dilution. Conversely, compounds **2**, **4**, **9**, and **11** produced a gradual recovery of activity over time. This curved jump dilution profile is characteristic of reversible-covalent inhibition,[53,82] and the enzyme–inhibitor dissociation rates (k_{-2}) of these four compounds were determined by nonlinear regression (eqn (4), Fig. 9 and Table 2).

Based on these data, the inhibition mechanism of each compound was classified as rapid-equilibrium (**1**, **3**, **6**, **8**), reversible-covalent (**2**, **4**, **5**, **9–11**), or irreversible-covalent (**7**). The rapid-equilibrium inhibitors may form either non-covalent or highly labile covalent interactions but were nonetheless approximated to a single-step mechanism (Fig. 9). The covalent inhibitors are defined by a two-step mechanism, in which initial non-covalent binding is followed by prolonged covalent bond formation. Reversible- and irreversible-covalent interactions are distinguished by the dissociation rate (k_{-2}) of the covalent bond (Fig. 9). Each inhibition mechanism is defined by a distinct inhibition constant (K_i, K_i^*, or K_I), obtained by fitting progress curves to the appropriate mechanism-specific regression model. Although these constants do not represent the same equilibrium, they provide a practical basis for comparing inhibitor potency.[78,83,84] Importantly, all inhibition constants were calculated assuming competitive binding with G6P at the active site. This is consistent with the reported mechanism of PLP, a known aryl aldehyde inhibitor of G6PD,[77,78] as well as estimated pK_a values, which show that G6P-binding Lys21 and Lys343 are the most nucleophilic lysine residues (pK_a = 10.4 and 10.3, respectively) in the protein sequence (average pK_a = 11.7, Table S3).

Table 2 summarizes inhibition constants derived from the fitted progress curves. Each dataset was fitted using a mechanism-specific regression model, corresponding to the mechanism previously assigned based on jump dilution experiments and progress curve shapes (Fig. S31–S33). Using benzaldehyde as a reference (**1**, $K_i = 616 \pm 2$ μM), salicylaldehyde (**3**) was nearly 2 orders of magnitude more potent ($K_i = 14 \pm < 1$ μM). 2-Ethynylbenzaldehyde (**7**) was also a strong inhibitor ($K_I = 53 \pm < 1$ μM). Compounds **4–6** showed moderate potency, with inhibition constants ranging from about 100–350 μM. In contrast, 4-pyridinecarboxaldehyde (**2**) and aryl aldehydes bearing negatively charged *ortho*-substituents (**8–11**) were poor inhibitors, with only millimolar activity. 2-Carboxybenzaldehyde (**10**) was the least potent with a K_i^* above 7.7 mM, exceeding its range of solubility.

Beyond inhibition constants, progress curves also permit evaluation of the association kinetics of covalent inhibitors. The regression model used for the irreversible-covalent inhibitor, 2-ethynylbenzaldehyde (**7**), provided a good fit for the association rate constant (k_2) of this compound (Table 2, $k_2 = 2.68 \pm 0.23 \times 10^{-4}$ s^{-1}). This value is comparable to a reported inhibitor of ABL protein kinase, which features **7** as a warhead appended onto an optimized non-covalent scaffold ($k_2 = 5.54 \times 10^{-3}$ s^{-1}).[27] The inactivation efficiency (k_2/K_I) of **7** against *L. mesenteroides* G6PD is therefore $5.1 \pm 0.5 \times 10^{-6}$ μM^{-1} s^{-1}. For the reversible-covalent inhibitors **2**, **5**, and **9**, k_2 was too slow to

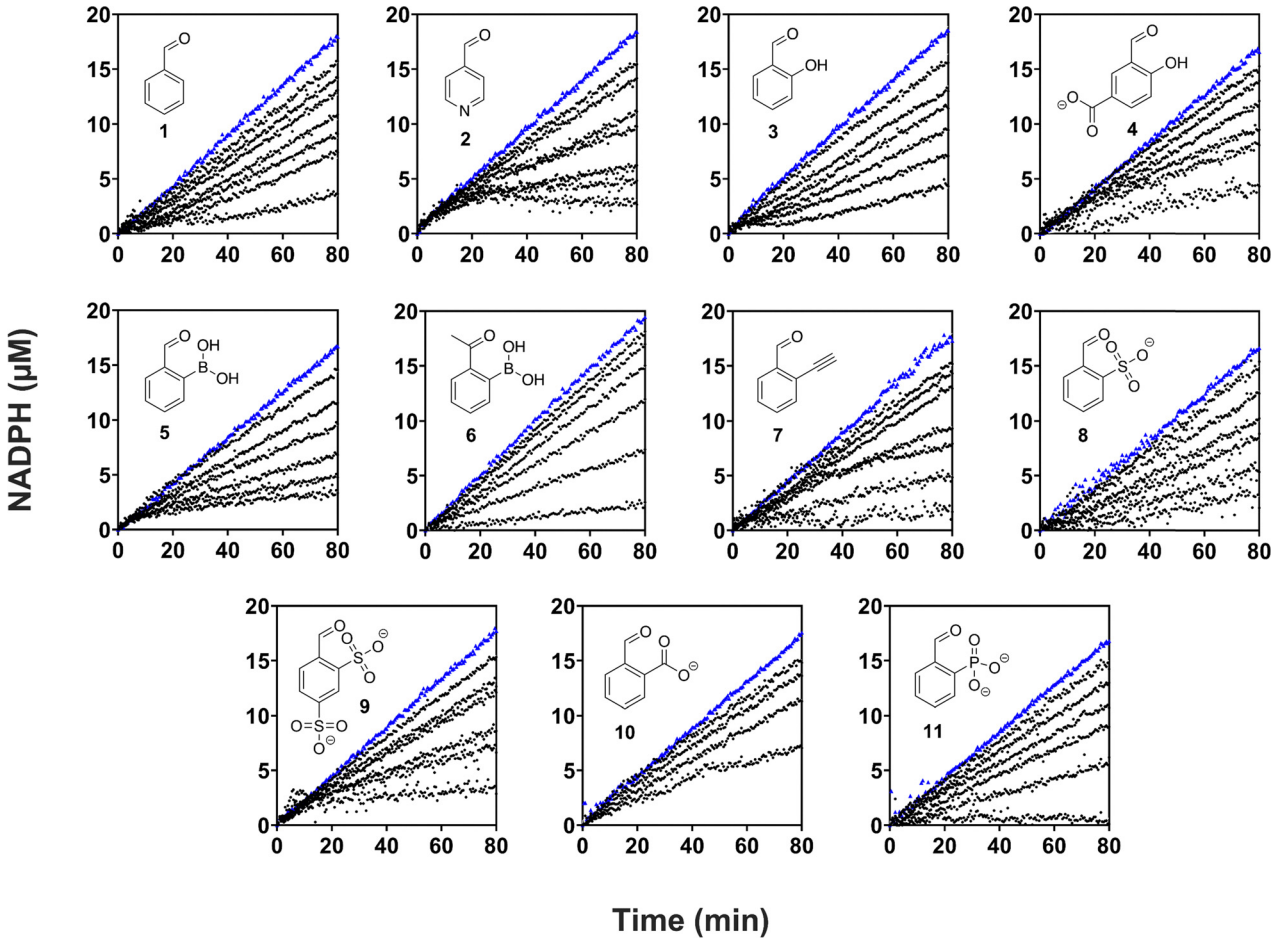

Fig. 7 Progress curves of aryl aldehyde inhibitors. *L. mesenteroides* G6PD activity was monitored in MOPS buffer (pH 7.4) by measuring NADPH production at varying inhibitor concentrations. Progress curve shape (biphasic *vs.* linear) informs inhibition mechanism. Black circles (●) are inhibited progress curves, blue triangles (▲) are uninhibited control reactions. Details on the concentrations used for each compound are provided in Fig. S31–S33. G6PD inhibition by compound **10** was limited within its range of solubility. Data shown correspond to one replicate.

quantify on the experimental timescale ($k_2 \gg k_{-2}$). This slow association is reflected in their progress curves, where the observed v_is are similar in rate to the v_{ctrl} (Fig. 7), described by Morrison and Walsh as an initial "burst" followed by a slower steady-state rate.[85] In contrast, the varied v_is observed for reversible-covalent inhibitors **4** and **11** indicates faster association kinetics. Estimation of k_2 typically relies on plotting k_{obs}, derived from progress curve fitting, against inhibitor concentration. However, this approach is sensitive to experimental noise and frequently error-prone.[54] As a result, reliable estimation of k_2 from the experimental data was not possible for compounds **4** and **11**.

Dissociation rate constants for the covalent inhibitors were derived from nonlinear regression of their jump dilution profiles, detailed in Table 2. The k_{-2} of 2-ethynylbenzaldehyde (**7**) was effectively zero as it is an irreversible-covalent inhibitor. Among the reversible-covalent inhibitors, compound **5** displayed the fastest dissociation kinetics, approaching those of a rapid-equilibrium inhibitor (Fig. 8). Compounds **9** (k_{-2} = 1.41 ± 0.06 s^{-1}) and **11** (k_{-2} = 0.18 ± 0.02 s^{-1}) demonstrated relatively moderate dissociation rates. In contrast, compounds **2** and **4** displayed slow dissociation kinetics, with only ~2% G6PD activity regained after 2 hours.

Discussion

ortho-Substituted aryl aldehydes have gained interest as imine-forming warheads for lysine-targeted covalent inhibitors. However, their development is limited by a lack of standardized structure–reactivity studies and systematic evaluation in enzyme systems. To address this gap, we mapped substituent effects onto imine formation using a lysine surrogate and then examined how these trends translate to pharmacodynamic outcomes in the inhibition of G6PD as a mechanistic model.

ortho-Substituents govern intrinsic reactivity

Imine formation across the *ortho*-substituted aryl aldehyde panel was primarily governed by two physicochemical factors: thermodynamic stabilization of the adduct and neighbouring group participation during bond formation. These determinants drove trends in product yield and rate, respectively, with

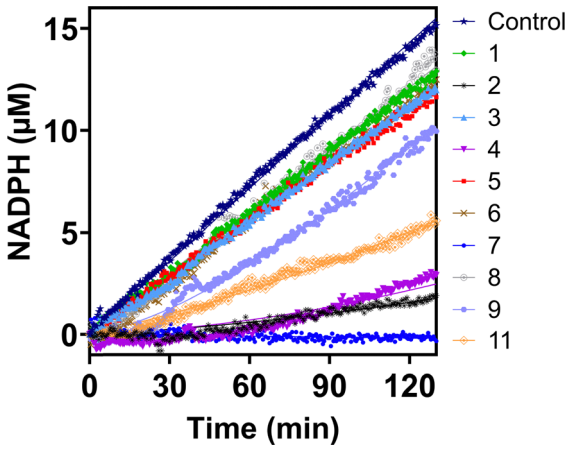

Fig. 8 Reversibility of aryl aldehyde inhibitors. *L. mesenteroides* G6PD was incubated with a high concentration of inhibitor (30 min, r.t.), and then rapidly diluted 50-fold with the addition of substrate. Reactions were conducted in MOPS buffer (pH 7.4) and G6PD activity was monitored my measuring NADPH formation. Linear curves with ~90% G6PD activity immediately recovered (compounds **1**, **3**, **5**, **6**, and **8**) represent rapid-equilibrium inhibition. Compounds that produce a gradual recovery of activity over time (**2**, **4**, **9** and **11**) are reversible-covalent inhibitors. These curves were fit by nonlinear least-squares regression to eqn (4) to derive k_{-2} values (Table 2). A linear curve with no recovered G6PD activity (compound **7**) reflects irreversible inhibition. Data shown correspond to one replicate.

A

$$E + I \underset{k_{-1}}{\overset{k_1}{\rightleftharpoons}} E\bullet I \underset{k_{-2}}{\overset{k_2}{\rightleftharpoons}} E\text{–}I$$

B

Inhibition Type	k_1	k_{-1}	k_2	k_{-2}	Inhibition Constant
Rapid-equilibrium	>0	>0	—	—	$K_i = \frac{k_{-1}}{k_1}$
Reversible covalent	>0	>0	>0	>0	$K_i^* = \frac{K_i}{1+\frac{k_2}{k_{-2}}}$
Irreversible covalent	>0	>0	>0	0	$K_I = K_i + \frac{k_2}{k_1}$

Fig. 9 Mechanisms of enzyme inhibition. (A) Binding equilibrium for two-step covalent inhibition. E = unbound enzyme, I = unbound inhibitor, E·I = non-covalent enzyme–inhibitor complex, E–I = covalent enzyme–inhibitor complex. (B) Kinetics of different inhibition mechanisms. Rapid-equilibrium inhibitors may form non-covalent or highly labile covalent interactions but were nonetheless approximated to a single-step mechanism (k_2 and k_{-2} do not apply). With the exception of slow-binding non-covalent inhibition, K_i is established effectively immediately, such that k_1 and k_{-1} are not rate-limiting.

additional substituents and competing reaction pathways further tuning observed reactivity.

Total imine yield was dictated by the degree of intramolecular stabilization imparted by the *ortho*-substituent, reflected by the parameter K_d^{app}. UV-Vis and NMR studies showed that 2-carbonylphenylboronic acids (**5**, **6**) had the highest apparent binding affinities and among the highest yields, consistent with the known formation of N–B dative bonds.[35] Hydroxyl-substituted salicylaldehydes (**3**, **4**) provide adduct stabilization through hydrogen bonds, although less effectively than N–B coordination, resulting in lower yields and K_d^{app} values. These observations align with previous work ranking these stabilization mechanisms in a similar system.[40] As expected for energetically stable products, imines formed by *ortho*-boronic acid and *ortho*-hydroxy aryl aldehydes were generally long-lived. Indeed, imines formed by 2-carbonylphenylboronic acids are known to be stable in aqueous solution for a week or longer.[35] In contrast, compounds with negatively charged *ortho*-substituents (**8**–**11**) showed little to no imine formation with Boc-Lys, suggesting that any putative n → π* contribution provides insufficient stabilization under our experimental conditions. While imine formation has been reported for **8**–**11** in aqueous solution, these reactions have required basic conditions or the use of amines more nucleophilic than Boc-Lys, such as cholamine or ethanolamine.[23,36,39] Overall, these findings correspond with estimated stabilization energies imparted by the N–B dative bond (−7.4 kcal mol^{-1}),[35] H-bond (−3.0 kcal mol^{-1}),[34] or n → π* interaction (−1.32 kcal mol^{-1} for **10**).[36]

ortho-Substituents also influenced reaction rate, as indicated by the UV-vis data. 2-Carbonylphenylboronic acids reacted rapidly with Boc-Lys within the reaction set-up time (1–2 min), whereas salicylaldehydes required longer equilibration times, and the ethynyl analogue was the slowest. These rate differences do not reflect predictions based on classical steric or electronic effects. Instead, these trends are more consistent with neighbouring group participation, where the *ortho*-substituent coordinates the aldehyde to promote a transition state-like geometry, thereby lowering the kinetic barrier.[86] Accelerated condensation reactions are well-documented for 2-carbonylphenylboronic acids, where the boron acts as a Lewis acid to coordinate the carbonyl oxygen for nucleophilic attack.[35] Hydroxyl groups on salicylaldehydes provide similar organizational effects through H-bonding, although less effectively.[35,87,88] In contrast, an ethynyl substituent is unable to engage in neighbouring group participation, resulting in relatively slow reaction rates despite minimal steric interference. Within individual *ortho*-substituent classes, we observed steric and electronic effects from additional substituents to fine-tune reaction rates, which has been examined in more detail elsewhere.[13,39,42,87]

Certain compounds deviated from thermodynamic expectations due to competing pathways that perturb the aldehyde-imine equilibrium. Notably, 2-ethynylbenzaldehyde (**7**) produced high product yields despite a low apparent binding affinity. This discrepancy arises from cyclization of the imine to form an isoquinolinium species that is highly stabilized by aromaticity.[27,37] As the imine is depleted, the K_d^{app} value of **7** becomes inflated over time. Salicylaldehyde (**3**) also showed evidence of a competing pathway, where the imine appeared to slowly hydrolyze after formation. This observation, however, contrasts with a similar study that monitored imine formation

Table 2 Kinetics of aryl aldehyde inhibition of *L. mesenteroides* G6PD

		Rate constant[a]		Inhibition constant[a]		
Aryl aldehyde	Inhibition type	k_2 (s^{-1})	k_{-2} (s^{-1})	K_i (μM)	K_i^* (μM)	K_I (μM)
1	Rapid-equilibrium	—	—	616 (± 2)	—	—
2	Reversible-covalent	$\gg k_{-2}$	0.07 (± <0.01)	—	2493 (± 9)	—
3	Rapid-equilibrium	—	—	14 (± <1)	—	—
4	Reversible-covalent	n.d.[b]	0.14 (± 0.01)	—	135 (± <1)	—
5	Reversible-covalent	$\gg k_{-2}$	→ ∞[c]	—	343 (± 1)	—
6	Rapid-equilibrium	—	—	369 (± 1)	—	—
7	Irreversible-covalent	2.68 (± 0.23) × 10^{-4}	→ 0	—	—	53 (± <1)
8	Rapid-equilibrium	—	—	4451 (± 6)	—	—
9	Reversible-covalent	$\gg k_{-2}$	1.41 (± 0.06)	—	1172 (± 3)	—
10	Reversible-covalent	—	n.d.[b]	—	>7700	—
11	Reversible-covalent	n.d.[b]	0.18 (± 0.02)	—	2938 (± 19)	—

[a] Data reported as parameter estimates ± SE, derived from nonlinear least-squares regression of one experimental replicate. [b] n.d. = not determined. [c] Dissociation kinetics of **5** were rapid, occurring nearly instantly on the experimental timescale.

and persistence for compound **3** over 12 hours by NMR.[42] These observations highlight the limitations of the equilibrium model used to determine K_d (aldehyde + amine ↔ imine), which assumes the reaction is a reversible, closed system yielding stable products. Furthermore, while UV-vis spectroscopy is a rapid and sensitive technique compared to NMR, it provides limited structural insight. As a potential alternative, LC-MS could improve the identification of species in the reaction mixture while maintaining reasonable acquisition times for time-dependent analyses. Similar HPLC-based assays with cysteine surrogates such as glutathione have been used to assess the reactivity of cysteine-targeting electrophiles.[89–91]

Mechanistic diversity in the inhibition of G6PD

Although the reactivity of aryl aldehyde electrophiles was largely governed by *ortho*-substituents, additional factors, such as binding site constraints, appeared to influence trends in potency and reversibility in the inhibition of *L. mesenteroides* G6PD.

The potency of tested aryl aldehyde inhibitors likely reflects a balance between electrophile reactivity and productive engagement within the enzyme binding pocket. Inhibition constants derived from fitted progress curves show that potency trends generally followed expected structure–reactivity relationships. *ortho*-Substituents that promoted relatively rapid and stable imine formation in the Boc-Lys system (hydroxyl, boronic acid, and ethynyl groups) also promoted stronger enzyme inhibition. These results are consistent with inhibition being driven by covalent engagement with the protein.[92–94] However, compared to reactions in bulk solvent, the enzyme binding pocket imposes additional steric and electrostatic constraints that modulate overall potency. For example, the 2-carbonylphenylboronic acids (**5**, **6**) had strong binding affinities and rapid reaction rates with Boc-Lys in solution, but were only moderate enzyme inhibitors. Relative to hydroxyl or ethynyl *ortho*-substituents, the large size of boronic acid may hinder access to the G6PD active site or constrain carbonyl alignment with lysine side-chains, partially offsetting its intrinsic physicochemical advantages. We imagine a similar penalty for the bulkier, charged aryl aldehyde *ortho*-substituents, compounded by electrostatic repulsion within the charged active site of G6PD.

Beyond inhibitory potency, the aryl aldehyde panel also showed substantial diversity in reversibility, as demonstrated by jump dilution experiments. However, *ortho*-substituents did not appear to drive these mechanistic trends. Compound **7** acted irreversibly, while compounds **2**, **4**, and **5** displayed reversible-covalent inhibition, consistent with behaviour reported in other enzyme systems.[27,29,31,95,96] We also observed reversible-covalent inhibition for compounds **9–11**, whose function as enzyme inhibitors has rarely been demonstrated.[23,36,39,97] Among these, a particularly compelling warhead is 2-formylphenylphosphonic acid (**11**). Its *ortho*-phosphonate group may demonstrate broader application, as many enzymes bind substrate phosphate groups through lysine residues. Potential targets include cancer-promoting tyrosine kinases,[98,99] viral DNA polymerases,[100,101] and RecA, which is associated with bacterial resistance.[102,103] In contrast, compounds **1**, **3**, **6**, and **8** behaved as rapid-equilibrium inhibitors of G6PD. Whether mediated by non-covalent interactions or highly labile covalent bonds, their inhibition involves a short residence time with the target. For salicylaldehyde (**3**) and 2-acetylphenylboronic acid (**6**), this rapid reversibility differs with behaviour reported in other enzyme systems.[31,35,104]

As an initial exploration of aryl aldehyde warheads as inhibitors of *L. mesenteroides* G6PD, these findings demonstrate functional activity while also revealing mechanistic diversity that warrants further investigation. Salicylaldehyde (**3**) showed an unexpectedly short residence time compared to its carboxyl-substituted derivative (**4**) despite a high potency and intrinsic capacity for imine stabilization. Similar discrepancies in reversibility were observed between the 2-carbonylphenylboronic acids (**5**, **6**) and the *ortho*-sulfonate-substituted aryl aldehydes (**8**, **9**). Another notable observation was the prolonged residence time of 4-pyridinecarboxaldehyde (**2**), despite the lack of a stabilizing *ortho*-substituent. This behaviour could stem from coenzyme pocket binding given its structural resemblance to the nicotinamide moiety of $NADP^+$. Interpretation of the observed mechanistic diversity may, therefore, be limited by the assumption that inhibition occurs exclusively through covalent modification within the G6P binding site. Substrate protection studies would help confirm proposed binding

mechanisms, while intact protein mass spectrometry could validate covalent adduct formation. For a more rigorous analysis of inhibitor binding kinetics, surface plasmon resonance is powerful technique for directly measuring association and dissociation rates.[31,105,106]

Tunable lysine-targeting inhibitors

To the best of our knowledge, PLP is the only reported G6PD inhibitor that uses an *ortho*-substituted aryl aldehyde as a covalent warhead. Here, we identified additional aryl aldehydes with previously unrecognized inhibitory activity against G6PD. Studies of G6PD from *L. mesenteroides*,[74,77,107] as well as *Homo sapiens*,[76] *Candida utilis*,[108] *Saccharomyces cerevisiae*,[109] and *Pseudomonas fluorescens*[110] consistently show that PLP forms an imine with an active-site lysine residue, competing with G6P binding. In *L. mesenteroides* G6PD, PLP selectively modifies Lys21 or Lys343, binding in an inverted orientation relative to G6P in the active site (Fig. 6B).[107] Although either residue can act as the nucleophile, only one molecule of PLP is bound per subunit in the fully inactivated enzyme.[77] We hypothesize that the aryl aldehydes in our panel predominantly modify the same residues implicated in PLP-mediated inhibition of *L. mesenteroides* G6PD. Support for this proposal is strongest for 3-formyl-4-hydroxybenzoic acid (**4**), which shares a salicylaldehyde scaffold, reversible-covalent mechanism, and comparable potency to PLP ($K_i^* = 135 \pm$ < 1 μM and 60 μM, respectively).[77] Lysine labelling studies such as LC-MS/MS peptide mapping or protein mass spectrometry will be required to confirm residue modification.

More broadly, our findings reveal substantial physicochemical and pharmacodynamic diversity among the tested aryl aldehydes, much of which arises from *ortho*-substituents. Tunability is useful in inhibitor design as it allows structure-based tailoring of drug properties, such as onset, duration of action, or selectivity, according to the therapeutic context (chronic or acute disease) or the targeted amine (buried or surface residue, high or low nucleophilicity).[6,55] Carbonyl-based warheads have previously been used to tune lysine-targeted inhibition of phosphatidylinositol-3-kinase-δ, optimizing physicochemical and pharmacodynamic properties such as reaction rate, reversibility, potency, selectivity, and toxicity.[22,111,112] While preliminary, our results support the development of aryl aldehydes as versatile lysine-targeting warheads for rational drug design. The most relevant biological context for this work is likely *H. sapiens* G6PD, which is a key metabolic regulator in humans and an emerging therapeutic target for cancer and inflammatory disease.[113]

Conclusions

The *ortho*-substituted aryl aldehydes studied in this work represent promising imine-forming warheads whose inhibitory activity is amenable to structure-based rational tuning. Here, we linked *ortho*-substituent effects governing imine formation with Boc-Lys to pharmacodynamic outcomes in our model enzyme, *L. mesenteroides* G6PD. *ortho*-Substituents that provided strong imine stabilization and engaged in neighbouring group participation produced high imine yields at faster rates. The reactivity of tested aryl aldehydes correlated in turn with inhibitory potency against G6PD. However, the reversibility of this inhibition appeared to be driven by other factors, such as the binding pocket microenvironment, rather than the *ortho*-substituent. Overall, this work provides an electrophile-first framework for advancing the design of novel, lysine-targeting covalent inhibitors, and highlights the apparent tunability of these warheads, which may be exploited to target a wide array of enzymes.

Author contributions

B. E. R: investigation, formal analysis, methodology, visualization, validation, data curation, conceptualization, writing – original draft, writing – review & editing. K. D. R: investigation, formal analysis, visualization, validation, data curation. A. A.: investigation, methodology, visualization, writing – review & editing. M. B: investigation, formal analysis, visualization. T. K: investigation, formal analysis, visualization. J. C. F.: methodology. A. J. N.: methodology. E. O.: methodology. D. L. J.: supervision, project administration, funding acquisition, conceptualization, methodology, resources, writing – review & editing.

Conflicts of interest

There are no conflicts to declare.

Data availability

The materials, methods and data supporting this article have been included as part of the supplementary information (SI), including synthetic procedures and characterization, NMR and UV-vis spectra of imine formation reactions, calculation procedure for total imine yields, enzyme kinetics, additional figures concerning the calculation of dissociation rates and inhibition constants, and estimated lysine pK_a values. See DOI: https://doi.org/10.1039/d6cb00070c.

Acknowledgements

This research was financially supported by the Natural Sciences and Engineering Research Council (NSERC), the Canadian Institute of Health Research (CIHR), and a Killam Predoctoral Scholarship (B. Rowland).

References

1 L. Hillebrand, X. J. Liang, R. A. M. Serafim and M. Gehringer, *J. Med. Chem.*, 2024, **67**, 7668–7758.
2 N. V. Mehta and M. S. Degani, *Drug Discovery Today*, 2023, **28**, 1–39.
3 L. Boike, N. J. Henning and D. K. Nomura, *Nat. Rev. Drug Discovery*, 2022, **21**, 881–898.

4 C. Gai, S. J. Harnor, S. Zhang, C. Cano, C. Zhuang and Q. Zhao, *RSC Med. Chem.*, 2022, **13**, 1460–1475.
5 S. De Cesco, J. Kurian, C. Dufresne, A. K. Mittermaier and N. Moitessier, *Eur. J. Med. Chem.*, 2017, **138**, 96–114.
6 M. You, H. Liu and C. Li, *JACS Au*, 2025, **5**, 5866–5887.
7 W. Lu, M. Kostic, T. Zhang, J. Che, M. P. Patricelli, L. H. Jones, E. T. Chouchani and N. S. Gray, *RSC Chem. Biol.*, 2021, **2**, 354–367.
8 L. K. Mader, J. E. Borean and J. W. Keillor, *RSC Med. Chem.*, 2025, **16**, 63–76.
9 D. Patel, Z. E. Huma and D. Duncan, *ACS Chem. Biol.*, 2024, **19**, 824–838.
10 R. Basu and S. Fletcher, *RSC Chem. Biol.*, 2026, 1–24.
11 F. Huang, X. Han, X. Xiao and J. Zhou, *Molecules*, 2022, **27**, 7728.
12 L. A. Highbarger, J. A. Gerlt and G. L. Kenyon, *Biochemistry*, 1996, **35**, 41–46.
13 C. Godoy-Alcántar, A. K. Yatsimirsky and J.-M. Lehn, *J. Phys. Org. Chem.*, 2005, **18**, 979–985.
14 G. Tang, W. Wang, X. Wang, K. Ding, S. C. Ngan, J.-Y. Chen, S. K. Sze, L. Gao, P. Yuan, X. Lu and S. Q. Yao, *Eur. J. Med. Chem.*, 2023, **259**, 1–24.
15 P. Udompholkul, C. Baggio, L. Gambini, G. Alboreggia and M. Pellecchia, *J. Med. Chem.*, 2021, **64**, 16147–16158.
16 J. Pettinger, M. Carter, K. Jones and M. D. Cheeseman, *J. Med. Chem.*, 2019, **62**, 11383–11398.
17 T. Tamura, T. Ueda, T. Goto, T. Tsukidate, Y. Shapira, Y. Nishikawa, A. Fujisawa and I. Hamachi, *Nat. Commun.*, 2018, **9**, 1–12.
18 M. Kawano, S. Murakawa, K. Higashiguchi, K. Matsuda, T. Tamura and I. Hamachi, *J. Am. Chem. Soc.*, 2023, **145**, 26202–26212.
19 P. A. Smith, M. F. T. Koehler, H. S. Girgis, D. Yan, Y. Chen, Y. Chen, J. J. Crawford, M. R. Durk, R. I. Higuchi, J. Kang, J. Murray, P. Paraselli, S. Park, W. Phung, J. G. Quinn, T. C. Roberts, L. Rougé, J. B. Schwarz, E. Skippington, J. Wai, M. Xu, Z. Yu, H. Zhang, M.-W. Tan and C. E. Heise, *Nature*, 2018, **561**, 189–194.
20 U. P. Dahal, A. M. Gilbert, R. S. Obach, M. E. Flanagan, J. M. Chen, C. Garcia-Irizarry, J. T. Starr, B. Schuff, D. P. Uccello and J. A. Young, *Med. Chem. Commun.*, 2016, **7**, 864–872.
21 S. E. Dalton, L. Dittus, D. A. Thomas, M. A. Convery, J. Nunes, J. T. Bush, J. P. Evans, T. Werner, M. Bantscheff, J. A. Murphy and S. Campos, *J. Am. Chem. Soc.*, 2018, **140**, 932–939.
22 B. Yuan, M. Ma, Y. Wu, J. Liu, M. Chen, Y. Lai, S.-Q. Zhang and M. Xin, *Eur. J. Med. Chem.*, 2025, **297**, 1–14.
23 M. V. V. Duro, K. S. Alnajjar, J. B. Sweasy, B. A. Kashemirov and C. E. McKenna, *Phosphorus, Sulfur Silicon Relat. Elem.*, 2019, **194**, 313–314.
24 T. Yang, A. Cuesta, X. Wan, G. B. Craven, B. Hirakawa, P. Khamphavong, J. R. May, J. C. Kath, J. D. Lapek, S. Niessen, A. L. Burlingame, J. D. Carelli and J. Taunton, *Nat. Chem. Biol.*, 2022, **18**, 934–941.
25 A. Bandyopadhyay, K. A. McCarthy, M. A. Kelly and J. Gao, *Nat. Commun.*, 2015, **6**, 1–9.
26 S. Asano, J. T. Patterson, T. Gaj and C. F. Barbas III, *Angew. Chem., Int. Ed.*, 2014, **53**, 11783–11786.
27 P. Chen, G. Tang, C. Zhu, J. Sun, X. Wang, M. Xiang, H. Huang, W. Wang, L. Li, Z.-M. Zhang, L. Gao and S. Q. Yao, *J. Am. Chem. Soc.*, 2023, **145**, 3844–3849.
28 P. Chen, J. Sun, C. Zhu, G. Tang, W. Wang, M. Xu, M. Xiang, C.-J. Zhang, Z.-M. Zhang, L. Gao and S. Q. Yao, *Angew. Chem., Int. Ed.*, 2022, **61**, 1–9.
29 D. Quach, G. Tang, J. Anantharajan, N. Baburajendran, A. Poulsen, J. L. K. Wee, P. Retna, R. Li, B. Liu, D. H. Y. Tee, P. Z. Kwek, J. K. Joy, W.-Q. Yang, C.-J. Zhang, K. Foo, T. H. Keller and S. Q. Yao, *Angew. Chem., Int. Ed.*, 2021, **60**, 17131–17137.
30 B. Metcalf, C. Chuang, K. Dufu, M. P. Patel, A. Silva-Garcia, C. Johnson, Q. Lu, J. R. Partridge, L. Patskovska, Y. Patskovsky, S. C. Almo, M. P. Jacobson, L. Hua, Q. Xu, S. L. I. Gwaltney, C. Yee, J. Harris, B. P. Morgan, J. James, D. Xu, A. Hutchaleelaha, K. Paulvannan, D. Oksenberg and Z. Li, *ACS Med. Chem. Lett.*, 2017, **8**, 321–326.
31 G. Akçay, M. A. Belmonte, B. Aquila, C. Chuaqui, A. W. Hird, M. L. Lamb, P. B. Rawlins, N. Su, S. Tentarelli, N. P. Grimster and Q. Su, *Nat. Chem. Biol.*, 2016, **12**, 931–936.
32 I. M. Bell, S. M. Stirdivant, J. Ahern, J. C. Culberson, P. L. Darke, C. J. Dinsmore, R. A. Drakas, S. N. Gallicchio, S. L. Graham, D. C. Heimbrook, D. L. Hall, J. Hua, N. R. Kett, A. S. Kim, M. Kornienko, L. C. Kuo, S. K. Munshi, A. G. Quigley, J. C. Reid, B. W. Trotter, L. H. Waxman, T. M. Williams and C. B. Zartman, *Biochemistry*, 2005, **44**, 9430–9440.
33 A. C. Eliot and J. F. Kirsch, *Annu. Rev. Biochem.*, 2004, **73**, 383–415.
34 J. Crugeiras, A. Rios, E. Riveiros and J. P. Richard, *J. Am. Chem. Soc.*, 2009, **131**, 15815–15824.
35 P. M. S. D. Cal, J. B. Vicente, E. Pires, A. V. Coelho, L. F. Veiros, C. Cordeiro and P. M. P. Gois, *J. Am. Chem. Soc.*, 2012, **134**, 10299–10305.
36 H. Chen, H. Ye, Y. Hai, L. Zhang and L. You, *Chem. Sci.*, 2020, **11**, 2707–2715.
37 P. N. Anderson and J. T. Sharp, *J. Chem. Soc., Perkin Trans. 1*, 1980, 1331–1334.
38 Y. Zhou, Q. Zhang, S. Jia, H. Ye and L. You, *Org. Lett.*, 2025, **27**, 2438–2443.
39 F. Esteve, T. Rieu and J.-M. Lehn, *Chem. Sci.*, 2024, **15**, 10408–10415.
40 A. Dal Corso, M. Catalano, A. Schmid, J. Scheuermann and D. Neri, *Angew. Chem., Int. Ed.*, 2018, **57**, 17178–17182.
41 S. Kulchat, M. N. Chaur and J.-M. Lehn, *Chem. – Eur. J.*, 2017, **23**, 11108–11118.
42 C. Delmas, E. Sager, C. Henry, U. Hassiepen, P. R. Skaanderup and I. Kerschgens, *Chimia*, 2025, **79**, 152–157.
43 F. Esteve, F. Rahmatova and J.-M. Lehn, *Chem. Sci.*, 2023, **14**, 10249–10257.
44 S. Jia, H. Ye and L. You, *Org. Chem. Front.*, 2022, **9**, 3966–3975.

45 G. J. Bartlett, C. T. Porter, N. Borkakoti and J. M. Thornton, *J. Mol. Biol.*, 2002, **324**, 105–121.
46 J. Pettinger, K. Jones and M. D. Cheeseman, *Angew. Chem., Int. Ed.*, 2017, **56**, 15200–15209.
47 M. E. Abbasov, M. E. Kavanagh, T.-A. Ichu, M. R. Lazear, Y. Tao, V. M. Crowley, C. W. Am Ende, S. M. Hacker, J. Ho, M. M. Dix, R. Suciu, M. M. Hayward, L. L. Kiessling and B. F. Cravatt, *Nat. Chem.*, 2021, **13**, 1081–1092.
48 S. M. Hacker, K. M. Backus, M. R. Lazear, S. Forli, B. E. Correia and B. F. Cravatt, *Nat. Chem.*, 2017, **9**, 1181–1190.
49 A. Krezel and W. Bal, *J. Inorg. Biochem.*, 2004, **98**, 161–166.
50 https://Supramolecular.org, https://supramolecular.org/bindfit, (accessed 19 November 2025).
51 P. Thordarson, *Chem. Soc. Rev.*, 2011, **40**, 1305–1323.
52 B. E. Rowland, J. C. Fuller, C. L. Okolie and D. L. Jakeman, *RSC Chem. Biol.*, 2026, DOI: 10.1039/D6CB00002A.
53 R. A. Copeland, A. Basavapathruni, M. Moyer and M. P. Scott, *Anal. Biochem.*, 2011, **416**, 206–210.
54 E. Mons, S. Roet, R. Q. Kim and M. P. C. Mulder, *Curr. Protoc.*, 2022, **2**, 1–85.
55 J. M. Bradshaw, J. M. McFarland, V. O. Paavilainen, A. Bisconte, D. Tam, V. T. Phan, S. Romanov, D. Finkle, J. Shu, V. Patel, T. Ton, X. Li, D. G. Loughhead, P. A. Nunn, D. E. Karr, M. E. Gerritsen, J. O. Funk, T. D. Owens, E. Verner, K. A. Brameld, R. J. Hill, D. M. Goldstein and J. Taunton, *Nat. Chem. Biol.*, 2015, **11**, 525–531.
56 J. Yang, R. A. Copeland and Z. Lai, *SLAS Discovery*, 2009, **14**, 111–120.
57 P. B. P. S. Reis, D.-A. Clevert and M. Machuqueiro, *Bioinformatics*, 2021, **38**, 297–298.
58 P. B. P. S. Reis, M. Bertolini, F. Montanari, W. Rocchia, M. Machuqueiro and D.-A. Clevert, *J. Chem. Theory Comput.*, 2022, **18**, 5068–5078.
59 C. E. Naylor, S. Gover, A. K. Basak, M. S. Cosgrove, H. R. Levy and M. J. Adams, *Acta Crystallogr., Sect. D:Biol. Crystallogr.*, 2001, **57**, 635–648.
60 M. Rad, S. Dehghanpour, S. Fatehfard, C. Gholamrezazadeh and A. Mahmoudi, *Polyhedron*, 2016, **106**, 10–17.
61 J.-R. Deng, N. C.-H. Lai, K. K.-Y. Kung, B. Yang, S.-F. Chung, A. S.-L. Leung, M.-C. Choi, Y.-C. Leung and M.-K. Wong, *Commun. Chem.*, 2020, **3**, 1–9.
62 Z. Li, L. Zhang, Y. Zhou, D. Zha, Y. Hai and L. You, *Eur. J. Org. Chem.*, 2022, 1–10.
63 I. Neira, A. Blanco-Gómez, J. M. Quintela, C. Peinador and M. D. García, *Org. Lett.*, 2019, **21**, 8976–8980.
64 M. Zheng, F.-J. Chen, K. Li, R. M. Reja, F. Haeffner and J. Gao, *J. Am. Chem. Soc.*, 2022, **144**, 15885–15893.
65 D. G. Isom, C. A. Castañeda, B. R. Cannon and B. García-Moreno E., *Proc. Natl. Acad. Sci. U. S. A.*, 2011, **108**, 5260–5265.
66 H. Ishikita, *FEBS Lett.*, 2010, **584**, 3464–3468.
67 R. Liu, Z. Yue, C.-C. Tsai and J. Shen, *J. Am. Chem. Soc.*, 2019, **141**, 6553–6560.
68 V. Fındık, B. T. Varınca Gerçik, Ö. Sinek, S. S. Erdem and M. F. Ruiz-López, *J. Chem. Inf. Model.*, 2022, **62**, 6775–6787.
69 N. Shindo, H. Fuchida, M. Sato, K. Watari, T. Shibata, K. Kuwata, C. Miura, K. Okamoto, Y. Hatsuyama, K. Tokunaga, S. Sakamoto, S. Morimoto, Y. Abe, M. Shiroishi, J. M. M. Caaveiro, T. Ueda, T. Tamura, N. Matsunaga, T. Nakao, S. Koyanagi, S. Ohdo, Y. Yamaguchi, I. Hamachi, M. Ono and A. Ojida, *Nat. Chem. Biol.*, 2019, **15**, 250–258.
70 S. M. Tomasio, H. P. Harding, D. Ron, B. C. S. Cross and P. J. Bond, *Mol. BioSyst.*, 2013, **9**, 2408–2416.
71 D. Spiegelberg, J. Stenberg, P. Richalet and M. Vanhove, *Eur. Biophys. J.*, 2021, **50**, 979–991.
72 J. Charoenpattarapreeda, Y. S. Tan, J. Iegre, S. J. Walsh, E. Fowler, R. S. Eapen, Y. Wu, H. F. Sore, C. S. Verma, L. Itzhaki and D. R. Spring, *Chem. Commun.*, 2019, **55**, 7914–7917.
73 A. Tantipanjaporn, J.-R. Deng, K.-H. A. Chan, K.-Y. K. Kung and M.-K. Wong, *Sens. Actuators, B*, 2025, **422**, 1–11.
74 C. Olive, M. E. Geroch and H. R. Levy, *J. Biol. Chem.*, 1971, **246**, 2047–2057.
75 M. S. Cosgrove, S. Gover, C. E. Naylor, L. Vandeputte-Rutten, M. J. Adams and H. R. Levy, *Biochemistry*, 2000, **39**, 15002–15011.
76 L. Camardella, C. Caruso, B. Rutigliano, M. Romano, G. Di Prisco and F. Descalzi-Cancedda, *Eur. J. Biochem.*, 1988, **171**, 485–489.
77 M. Milhausen and H. R. Levy, *Eur. J. Biochem.*, 1975, **50**, 453–461.
78 C. Zimmer, J. Brauer, D. Ferenc, J. Meyr, P. Müller, H.-J. Räder, B. Engels, T. Opatz and T. Schirmeister, *Molecules*, 2024, **29**, 1–16.
79 L. K. Mader and J. W. Keillor, *RSC Med. Chem.*, 2025, **16**, 2517–2531.
80 R. Copeland, *Evaluation of Enzyme Inhibitors in Drug Discovery: A Guide for Medicinal Chemists and Pharmacologists*, John Wiley & Sons, Ltd, Hoboken, 2nd edn, 2013, pp. 203–244.
81 S. Ludewig, M. Kossner, M. Schiller, K. Baumann and T. Schirmeister, *Curr. Top. Med. Chem.*, 2010, **10**, 368–382.
82 M. I. Ali and P. J. Tonge, *Br. J. Pharmacol.*, 2026, 1–12.
83 L. Agost-Beltrán, C. Zimmer, H. J. Räder, C. Kersten, T. Schirmeister, S. Rodríguez and F. V. González, *Bioorg. Chem.*, 2024, **153**, 1–16.
84 G. Wang, N. Moitessier and A. K. Mittermaier, *Chem. Commun.*, 2023, **59**, 10866–10882.
85 J. F. Morrison and C. T. Walsh, *Advances in Enzymology and Related Areas of Molecular Biology*, John Wiley & Sons, Inc., New York, 1988, vol. 61, pp. 201–301.
86 F. V. Lijsebetten, J. O. Holloway, J. M. Winne and F. E. D. Prez, *Chem. Soc. Rev.*, 2020, **49**, 8425–8438.
87 A. Jezierska-Mazzarello, H. Szatyłowicz and T. M. Krygowski, *J. Mol. Model.*, 2012, **18**, 127–135.
88 S. Cambray and J. Gao, *Acc. Chem. Res.*, 2018, **51**, 2198–2206.
89 L. Petri, P. Ábrányi-Balogh, P. R. Varga, T. Imre and G. M. Keserű, *Bioorg. Med. Chem.*, 2020, **28**, 1–7.
90 D. Yamane, R. Tetsukawa, N. Zenmyo, K. Tabata, Y. Yoshida, N. Matsunaga, N. Shindo and A. Ojida, *J. Med. Chem.*, 2023, **66**, 9130–9146.
91 S. Dong, H. Huang, J. Li, X. Li, S. J. Bunu, Y. Yang, Y. Zhang, Q. Jia, Z. Xu, Y. Li, H. Zhou, B. Li and W. Zhu, *Commun. Chem.*, 2024, **7**, 1–10.

92 J. A. H. Schwöbel, Y. K. Koleva, S. J. Enoch, F. Bajot, M. Hewitt, J. C. Madden, D. W. Roberts, T. W. Schultz and M. T. D. Cronin, *Chem. Rev.*, 2011, **111**, 2562–2596.
93 T. Zimmermann, E. Endres, C. Sotriffer and M. Decker, *ACS Med. Chem. Lett.*, 2024, **15**, 1708–1714.
94 R. A. Ward, M. J. Anderton, S. Ashton, P. A. Bethel, M. Box, S. Butterworth, N. Colclough, C. G. Chorley, C. Chuaqui, D. A. E. Cross, L. A. Dakin, J. É. Debreczeni, C. Eberlein, M. R. V. Finlay, G. B. Hill, M. Grist, T. C. M. Klinowska, C. Lane, S. Martin, J. P. Orme, P. Smith, F. Wang and M. J. Waring, *J. Med. Chem.*, 2013, **56**, 7025–7048.
95 C. D. Douglas, L. Grandinetti, N. M. Easton, O. P. Kuehm, J. A. Hayden, M. C. Hamilton, M. St. Maurice and S. L. Bearne, *Biochemistry*, 2021, **60**, 2508–2518.
96 P. Bandyopadhyay and S. Jha, *Prog. React. Kinet. Mech.*, 2013, **38**, 75–85.
97 M. V. V. Duro, PhD thesis, University of Southern California, 2021.
98 J. C. Lougheed, R.-H. Chen, P. Mak and T. J. Stout, *J. Biol. Chem.*, 2004, **279**, 44039–44045.
99 O. Hantschel, F. Grebien and G. Superti-Furga, *Cancer Res.*, 2012, **72**, 4890–4895.
100 S. Shankar, J. Pan, P. Yang, Y. Bian, G. Oroszlán, Z. Yu, P. Mukherjee, D. J. Filman, J. M. Hogle, M. Shekhar, D. M. Coen and J. Abraham, *Cell*, 2024, **187**, 5572–5586.e15.
101 J. Piret and G. Boivin, *The Enzymes*, Elsevier, London, 2021, vol. 50, pp. 79–132.
102 Z. Chen, H. Yang and N. P. Pavletich, *Nature*, 2008, **453**, 489–494.
103 T. J. Wigle, A. M. Lee and S. F. Singleton, *Biochemistry*, 2006, **45**, 4502–4513.
104 M. Mason, L. Belvisi, L. Pignataro and A. Dal Corso, *ChemBioChem*, 2024, **25**, 1–7.
105 C. F. Shuman, M. D. Hämäläinen and U. H. Danielson, *J. Mol. Recognit.*, 2004, **17**, 106–119.
106 W. Zhou, X. Ye, S. Pandey and X. Du, *ACS Omega*, 2025, **10**, 29637–29646.
107 J. R. LaDine, D. Carlow, W. T. Lee, R. L. Cross, T. G. Flynn and H. R. Levy, *J. Biol. Chem.*, 1991, **266**, 5558–5562.
108 H. J. Engel, W. Domschke, M. Alberti and G. F. Domagk, *Biochim. Biophys. Acta, Enzymol.*, 1969, **191**, 509–516.
109 M. T. Vincenzini, P. Vanni, G. M. Hanozet, P. Parenti and A. Guerritore, *Enzyme*, 1986, **36**, 239–246.
110 D. Lessmann and G. Kurz, *Biochem. Soc. Trans.*, 1975, **3**, 1061–1062.
111 B. Yuan, Y. Feng, M. Ma, W. Duan, Y. Wu, J. Liu, H.-Y. Zhao, Z. Yang, S.-Q. Zhang and M. Xin, *J. Med. Chem.*, 2024, **67**, 20076–20099.
112 B. Yuan, J. Liu, Y. Wu, M. Chen, Y. Lai, H.-Y. Zhao, Z. Yang, S.-Q. Zhang and M. Xin, *J. Med. Chem.*, 2025, **68**, 11437–11467.
113 A. Koperniku, A. A. Garcia and D. Mochly-Rosen, *J. Med. Chem.*, 2022, **65**, 4403–4423.